ELSEVIER

Journal of Non-Crystalline Solids 274 (2000) 313–318

JOURNAL OF NON-CRYSTALLINE SOLIDS

www.elsevier.com/locate/jnoncrysol

Electronic transport and optical properties of proton-implanted amorphous $2CdO \cdot GeO_2$ films

S. Narushima [a,*], H. Hosono [a], J. Jisun [b], T. Yoko [b], K. Shimakawa [c]

[a] *Materials and Structures Laboratory, Tokyo Institute of Technology, Nagatsuta, Yokohama 226-8503, Japan*
[b] *Institute for Chemical Research, Kyoto University, Uji, Kyoto 611, Japan*
[c] *Department of Electronics, Gifu University, Gifu 501-11, Japan*

Abstract

Films of amorphous $2CdO \cdot GeO_2$ with the band gap of 3.4 eV were prepared by rf sputtering. Protons were implanted into the films at doses 2×10^{14}–2×10^{16} cm^{-2}. On going from 2×10^{14} to 2×10^{16} cm^{-2}, dc conductivity at 300 K increased from $\sim 10^{-9}$ to $\sim 10^{1}$ S cm^{-1} and its activation energy fell from $\sim$ 1 eV to almost zero (degenerate state). This result indicates that the Fermi level of this amorphous material may be controlled by proton implantation. The sign of Hall and Seebeck coefficients were negative, showing n-type electrical conduction and no pn sign anomaly in Hall voltages. The Hall mobility was of the order of 10 cm^2 V^{-1} s^{-1} (even at carrier concentration of $\sim 3 \times 10^{19}$ cm^{-3}), which is larger by several orders of magnitude than that of existing amorphous semiconductors. No degradation of visible transparency was observed in all implanted samples. The optical conductivity may be described by the classical Drude formula with a single relaxation time, 2.7×10^{-15} s. X-ray radial distribution function revealed that the local structure around Cd^{2+} (coordination number; $\sim$ 6) and Ge^{4+} ($\sim$ 4) in the amorphous state is close to that of crystalline Cd_2GeO_4 and the amorphous state has a distribution of Cd–O–Cd bond angles. We assume that the electronic transport properties of the present material primarily originate from the extended conduction bands composed of Cd 5s orbitals. © 2000 Elsevier Science B.V. All rights reserved.

1. Introduction

Amorphous semiconductors have a long history comparable to crystalline semiconductors as indicated by the first report on V_2O_5-based amorphous oxide semiconductors by Denton et al. in 1954 [1]. Control of conductivity is difficult in amorphous semiconductors. Structural flexibility, which is favorable to the formation of the amorphous state, makes carrier generation efficiency by doping small [2].

Existing amorphous semiconductors have a common electronic transport property, which is not seen in crystalline semiconductors, i.e., sign anomaly in Hall effects [3]. The sign of Hall coefficient for p or n-type conductors is opposite to that of Seebeck coefficient. This difference is the primary reason for difficulty in obtaining fundamental physical parameters associated with electronic transport such as the effective mass and the mobility in our opinion.

We have explored a novel category of amorphous semiconductors, i.e., transparent amorphous semiconductors, following a working

* Corresponding author. Tel.: +81-45 924 5628; fax: +81-45 924 5339.
E-mail address: narushil@rlem.titech.ac.jp (S. Narushima).

0022-3093/00/$ - see front matter © 2000 Elsevier Science B.V. All rights reserved.
PII: S 0 0 2 2 - 3 0 9 3 (0 0) 0 0 1 9 4 - 0

hypothesis [4–6] which was deduced from a consideration of chemical bonding in oxides. Oxides were chosen as the basic system so as to obtain a wide band gap. As represented by V_2O_5-based oxide glass, amorphous oxides containing transition metal ions are obviously inappropriate because of coloring and resistivity owing to mobility $\sim 10^{-4}$ cm^2 V^{-1} s^{-1} [7]. To obtain larger electron mobilities, a larger overlap between relevant basis orbitals is required. Our working hypothesis is to explore metal oxides composed of heavy metal cations, which have an electronic configuration of $(n-1)d^{10}ns^0$ (where $n \geqslant 5$) as candidate materials. The bottom part of conduction band in these oxides is primarily composed of *n*s orbitals of the heavy metal cation. The spatial spreading of *n*s orbitals of heavy metal cations is larger than lighter cations and their shape is spherical. As a consequence, the magnitude of the overlap between neighboring *n*s orbitals are larger than those between relatively small s orbitals of light metal cations and is less affected by structural randomness in contrast to the case with p–p or d–p orbitals having spatial anisotropy.

Cd^{2+} and Ge^{4+} have the electronic configuration of $4d^{10}5s^0$ and $3d^{10}4s^0$, respectively. Corresponding crystalline phase of Cd_2GeO_4 has an olivine-type structure [8]. Thus amorphous (a-) $2CdO \cdot GeO_2$ meets the requirement of the above working hypothesis.

The purposes of this paper are: (1) to show that the Fermi level of a-$2CdO \cdot GeO_2$ can be changed by ion implantation of protons, (2) to examine optical properties of the implanted specimens and (3) to consider electronic transport properties of the material based on structural information.

2. Experimental procedures

Film specimens were deposited on synthetic silica glass substrates by radio frequency sputtering method using a sintered disk of polycrystalline Cd_2GeO_4 as a sputtering target [5]. The substrates were not heated during deposition. The thickness of as-deposited films was ~ 700 nm. Chemical compositions of the films were determined by inductively coupled plasma emission (ICP) spectroscopy after the samples were dissolved in acid solution. Protons were implanted into as-deposited specimens at ambient temperature at doses 2×10^{14}, 2×10^{15} and 2×10^{16} cm^{-2}. The specimens were wrapped with Al foil except portions to be implanted to avoid charging during implantation. To reduce the concentrations of implanted ions in the ion stopping regions, two accelerating voltages were employed for each implantation, for example, the total dose of 2×10^{16} cm^{-2} was 1×10^{16} cm^{-2} at 40 kV plus 1×10^{16} cm^{-2} at 70 kV. Depth profile of implanted protons was calculated using the transport of ions matter (TRIM-94) code [9]. The dose rate was ~ 0.2 μA cm^{-2} (2.4×10^{12} ions cm^{-2} s^{-1}). The amorphous state of resulting films was confirmed by glancing angle X-ray diffraction and selected area electron diffraction (SEED) patterns under cross-sectional transmission electron microscopy (TEM) observation.

Optical transmission spectra of the samples before and after ion implantation were measured with a spectrophotometer (Hitachi U4000) in the ultraviolet–visible-near infrared range at room temperature. DC electrical conductivity of the samples was measured as a function of temperature by either a four- or two-probe method depending on sample conductivity. The samples were placed in a cryostat equipped with helium refrigerator and the measurements were carried out over the temperature range between 13 and 300 K in vacuum ($\sim 10^{-5}$ Torr). Gold film was sputtered on the surface of the samples after H^+-implantation and was used as electrodes for electrical measurements. Ohmic contacts were confirmed over the temperature range. Hall effect was measured by Van der Pauw method at 300 K in a static magnetic field of 0.7 T. Thermopower was measured at 300 K using a film heater.

X-ray diffraction measurements on as-deposited films were carried out with Mo Kα radiation (50 kV–40 mA) from a diffractometer (Rigaku RINT 1200). The film thickness was ~ 15 μm and a flat plate of silica glass was used as a substrate. Scattering intensity was measured by step scanning method using a silicon solid state detector (Kevex Si-SSD) in an energy range of 17.37–17.71 keV. The fixed time and step angle were 200 s, 0.2° for $2\theta = 4$–23°, 400 s, 0.5° for 18–80°, and 600 s, 1.0°

for 75–150°, respectively. The incident angle was fixed at 2°. Diffraction angle, 2θ, ranged 4–150°, which corresponds to a scattering vector ($S = 4\pi \sin\theta/\lambda$) of 0.6–17 Å^{-1}.

After applying data corrections (absorption, polarization, air-scattering), the scattering data were normalized by Krogh-Moe–Norman method [10,11] and then an interference function, $S \cdot i(S)$, was calculated. The radial distribution function (RDF) was obtained by Fourier transform of $S \cdot i(S)$ to a maximum S of 17 Å^{-1}.

3. Results

Chemical compositions of the resulting samples were $63CdO \cdot 37GeO_2$. Since this composition is close to $2CdO \cdot GeO_2$, the composition of the samples is denoted as $2CdO \cdot GeO_2$, hereafter.

Fig. 1 shows changes in dc electrical conductivity of the samples upon H^+ ion implantation. Conductivity, σ, of as-deposited sample was of the order of 10^{-9} S cm^{-1}. Upon H^+-implantation, an increase of conductivity with dose, i.e., $\sigma = \sim 10^{-7}$ S cm^{-1} for 2×10^{14} cm^{-2}, $\sim 10^{-5}$ S cm^{-1} for 2×10^{15} cm^{-2} and $\sim 10^{1}$ S cm^{-1} for 2×10^{16} cm^{-2} at 300 K was observed. Fig. 1 also shows conductivity of the samples as a function of temperature. Temperature dependence of conductivity of the samples with dose of 2×10^{14} cm^{-2} or 2×10^{15} cm^{-2} was of thermal activation type. Conductivity of the sample implanted to 2×10^{16} cm^{-2} has a slightly negative slope of temperature dependence but remained almost constant down to 13 K. The activation energy of electrical conduction of the samples was calculated from the slope of the function $\ln\sigma = A + B/T$ fitted to the conductivity data with least square method. The correlation coefficients of the fits were > 0.97. As shown in Fig. 1, the activation energy, E_a, decreased with increasing dose, i.e., ~ 1 eV for 2×10^{14} cm^{-2}, ~ 0.06 eV for 2×10^{15} cm^{-2} and ~ 0 eV for 2×10^{16} cm^{-2}.

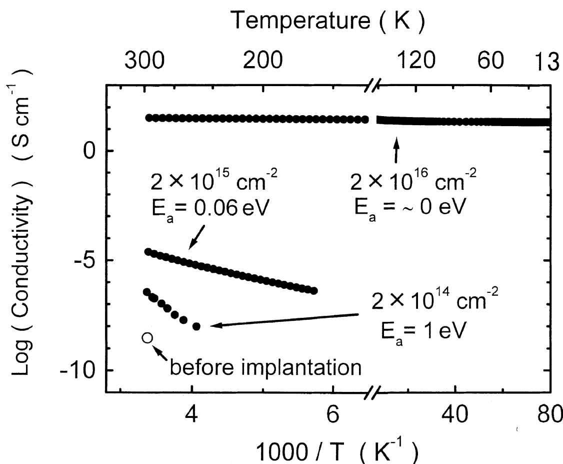

Fig. 1. DC electrical conductivity of amorphous $2CdO \cdot GeO_2$ films before and after implantation with H^+ ion to dose of 2×10^{14} cm^{-2}, 2×10^{15} cm^{-2} and 2×10^{16} cm^{-2} as a function of temperature. Note the axis break and change of horizontal scale.

Hall and Seebeck coefficients at 300 K of the sample implanted to a dose of 2×10^{16} cm^{-2} were $\sim -2 \times 10^{-1}$ cm^3 C^{-1} and ~ -60 μV K^{-1}, respectively. They were both negative, indicating n-type electrical conduction and no pn sign anomaly was observed. Hall mobility and carrier concentration at 300 K of the sample implanted to a dose of 2×10^{16} cm^{-2} were ~ 13 cm^2 V^{-1} s^{-1} and $\sim 3 \times 10^{19}$ cm^{-3}, respectively. No reliable data on the samples to doses $< 2 \times 10^{15}$ cm^{-2} were obtained due to large fluctuations in Hall voltages or in thermopower.

The samples are transparent and not colored in the visible region both before and after the implantation. Fig. 2 shows the optical transmission spectra of a sample before and after H^+-implantation (2×10^{16} cm^{-2}). None of the implanted samples had loss more than $\sim 3\%$ of transmittance in the visible range. Optical band gap for the as-deposited specimens, estimated from Tauc plots [12] of the optical absorption spectra, was ~ 3.4 eV. The implantation induced two changes in the optical spectrum, i.e., a blue shift of the absorption edge and a transmittance loss in near infrared region. The former and latter are ascribed to Burstein effect [13] (band filling by carrier electrons) and free carrier absorption, respectively. Inset in Fig. 2 shows the frequency (energy) dependent optical conductivity, $\sigma(\omega)$, obtained from the absorption coefficient and the fitted curve using the Drude formula $\sigma(\omega) = \sigma(0)/[1 + \omega^2\tau^2]$. $\sigma(\omega)$ is

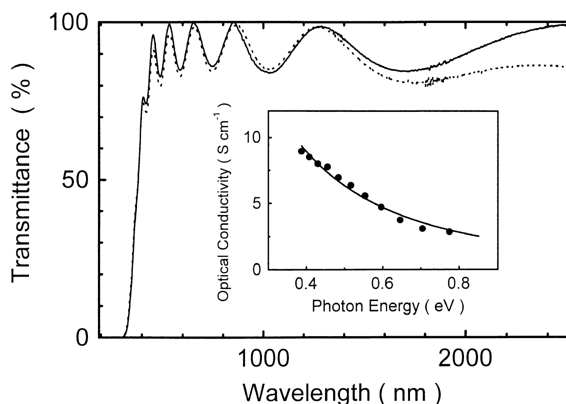

Fig. 2. Optical transmission spectra of amorphous $2CdO \cdot GeO_2$ films before (solid line) and after (dashed line) H^+-implantation (2×10^{16} cm^{-2}). The inset shows optical conductivity. Circles and solid line denote experimental data of the implanted specimen and a fit to the Drude formula, respectively.

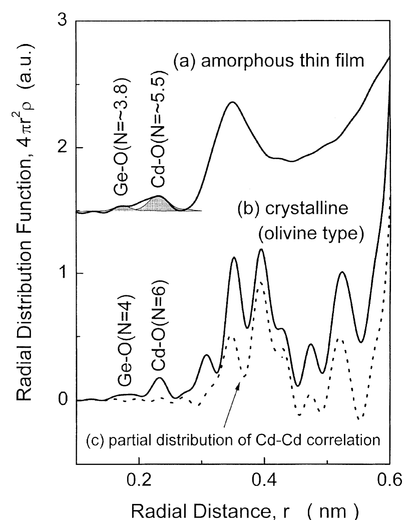

Fig. 3. Radial distribution functions (RDF): (a) experimentally observed RDF of amorphous $2CdO \cdot GeO_2$ film (solid line), and calculated partial pair correlation of cation-oxygen by pair function method (area filled line), (b) RDF of crystalline Cd_2GeO_4 calculated by pair function method, (c) partial distribution of Cd–Cd correlation in RDF of crystalline Cd_2GeO_4.

almost proportional to ω^{-2}, indicating that the system may be described by a single relaxation time $\tau(2.7 \times 10^{-15}$ s) [14].

Fig. 3 shows observed X-ray RDF along with calculated RDF of crystalline Cd_2GeO_4. Average coordination number of first neighboring O around cations for the amorphous state was estimated by pair function method [15] for the observed RDF. The obtained coordination numbers of O around Cd was ~ 5.5 and ~ 3.8 around Ge. The bond length between the cation and the oxygen was ~ 0.23 nm for Cd–O and ~ 0.17 nm for Ge–O. These lengths are almost the same as those reported in the crystalline form [8]. The calculated partial distribution of Cd–Cd correlation in the crystalline state is shown in Fig. 3(c). It indicates that RDF in the region ~ 0.4 nm is primarily dominated by the Cd–Cd correlation. The contribution of Cd–Ge is less because the atomic scattering factor of Cd is about 1.5 times larger than that of Ge [16]. It is evident from a comparison in the region ~ 0.4 nm between the RDF's of the amorphous and crystalline state that Cd–Cd correlation is lost in the amorphous state. No difference within errors exists in the Cd–O bond distance between the crystalline and amorphous state. As a consequence, the amorphous state has a distribution of Cd–O–Cd bond angles.

4. Discussion

Important results obtained here are: (1) the decrease in activation energy for the electrical conduction, i.e., ~ 1 eV to ~ 0 eV on going from dose $\sim 10^{14}$ to $\sim 10^{16}$ cm^{-2} implanted protons and (2) the electron mobility ~ 10 cm^2 V^{-1} s^{-1} and the absence of pn sign anomaly in Hall effect.

The continuous change in activation energy with implantation dose indicates that Fermi level in a-$2CdO \cdot GeO_2$ can be shifted in the range from insulating to degenerate state by H^+-implantation. The conductivity around 300 K is also shifted between $\sim 10^{-9}$ and $\sim 10^1$ S cm^{-1}. Amorphous $2CdO \cdot GeO_2$ with the conductivity of $\sim 10^1$ S cm^{-1} is due to degenerate state as evidenced by observation of Burstein effect even in the amorphous state. The carrier concentration at a dose of $\sim 10^{16}$ cm^{-2} implanted protons was $\sim 3 \times 10^{19}$ cm^{-3}. We assume that the generation of conduction carrier in the H^+-implanted a-$2CdO \cdot GeO_2$ would be progress of a chemical reaction, $H \to H^+ + e^-_{cond}$ and that the carrier doping with proton is of interstitial type. On assumption that

each implanted proton generates a conduction electron, the carrier generation efficiency, which is deduced from the carrier concentration of the sample to a dose of $\sim 10^{16}$ cm^{-2}, is $\sim$ 10%. The experimental results indicate that the proton implantation is efficient carrier doping method in a-$2CdO \cdot GeO_2$.

The mobility of degenerate state is $\sim$ 10 cm^2 V^{-1} s^{-1}, which is larger by several orders of magnitude than that of amorphous semiconductors (i.e., $\sim 10^{-4}$ cm^2 V^{-1} s^{-1} for amorphous As_2S_3 [17] and 10^{-1} cm^2 V^{-1} s^{-1} for hydrogenerated amorphous silicon [18]) and is almost the same as that in the polycrystalline form (the carrier mobility in crystalline Cd_2GeO_4 is $\sim$ 10 cm^2 V^{-1} s^{-1} [19]). We anticipate that such a large mobility originates from an extended electronic state at the bottom of conduction band [5]. It is interesting to note that optical conductivity can be fitted by the Drude formula with a single relaxation time (τ) as in crystalline state. The estimated τ provides the mean free path, l, of $\sim$ 1 nm (the procedure is described in Ref. [14]). This l is several times larger than the atomic distance and is close to those found for liquid metals [20].

Here, let us consider the origin of the large mobility in a-$2CdO \cdot GeO_2$ from structural aspects. The unique electric transport properties, such as mobility of $\sim$ 10 cm^2 V^{-1} s^{-1} or long mean free path $\sim$ 1 nm in the material indicate that the wide distribution of Cd–O–Cd bond angles due to the structural randomness in our samples, does not seriously affect the extended electronic state in the conduction band bottom. It is reported [21] that the bottom part of the conduction band is mainly composed of 5s orbitals of Cd^{2+}. Since the mobility is proportional to the width of the conduction band, the present results indicate that the magnitude of overlap between the 5s orbitals of the second neighboring Cd^{2+}s in the amorphous state is comparable to that in the crystalline state. Fig. 4 illustrates the schematic representation of orbital drawing for conduction band bottom. The magnitudes of overlap of the 5s orbitals of neighboring Cd^{2+}s between crystalline and amorphous state are compared. The spatial spreading of Cd^{2+}5s orbital is large and the shape is spherical. Thus, the magnitude of overlap between the 5s orbitals of neighboring Cd^{2+}s is relatively insensitive to the variation of the Cd–O–Cd bond angle, which is intrinsic to the amorphous state. As a consequence, a-$2CdO \cdot GeO_2$ has electronic transport properties similar to those of the crystalline state. The fact that optical conductivity may be described by the Drude formula using a single relaxation time substantiates this feature.

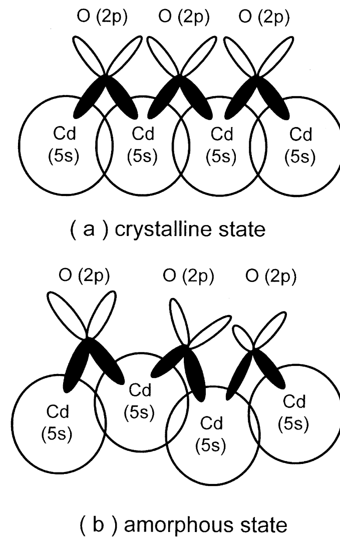

Fig. 4. Schematic representation of orbital drawing for conduction band bottom: (a) crystalline, (b) amorphous state.

5. Conclusions

1. The Fermi level of transparent amorphous $2CdO \cdot GeO_2$ may be controlled in the range from insulating to degenerate semiconducting state by proton implantation. DC electrical conductivity at 300K may be changed in the range $\sim 10^{-9}$ S cm^{-1} to $\sim 10^{1}$ S cm^{-1} (degenerate semiconductor).
2. The conduction type is n-type, and no pn sign anomaly of Hall coefficient was detected. The electron mobility is $\sim$ 10 cm^2 V^{-1} s^{-1}. This mobility is larger by several orders of magnitude than that of existing amorphous semiconductors and is almost the same as that in the polycrystalline form.
3. X-ray radial distribution function reveals that the local structure around Cd^{2+} (coordination

number; ∼ 6) and Ge^{4+} (∼ 4) in the amorphous state is close to that of crystalline state. The amorphous state has a distribution of Cd–O–Cd bond angle.

4. The optical conductivity could be described by the Drude formula assuming a single relaxation time.
5. We assume that the electronic transport properties primarily originate from the extended nature of the states at the conduction band bottom composed of spatially extended and spherical Cd 5s orbitals.

References

[1] E.D. Denton, H. Rawson, J. Stanworth, Nature 173 (1954) 1030.
[2] N.F. Mott, Philos. Mag. 19 (1969) 835.
[3] S.R. Elliott, Physics of Amorphous Materials, Longman, New York, 1983.
[4] M. Yasukawa, H. Hosono, N. Ueda, H. Kawazoe, Jpn. J. Appl. Phys. 34 (1996) L281.
[5] H. Hosono, N. Kukuchi, N. Ueda, H. Kawazoe, K. Shimizu, Appl. Phys. Lett. 67 (18) (1995) 2663.
[6] H. Hosono, Y. Yamashita, N. Ueda, H. Kawazoe, K. Shimizu, Appl. Phys. Lett. 68 (1996) 661.
[7] A. Vomvas, M. Roilos, Philos. Mag. B 49 (1984) 143.
[8] E.L. Belokoneva, et al., Sov. Phys. Crystallogr. 18 (1974) 610.
[9] J.F. Ziegler (Ed.), The Stopping and Range of Ions in Solids, Pergamon, New York, 1985.
[10] J. Krogh-Moe, Acta Crystallogr. 9 (1956) 351.
[11] N. Norman, Acta Crystallogr. 10 (1957) 370.
[12] J. Tauc, R. Grigorovici, A. Vancu, Phys. Stat. Sol. 15 (1966) 627.
[13] E. Burstein, Phys. Rev. 93 (1954) 632.
[14] K. Shimakawa, S. Narushima, H. Hosono, H. Kawazoe, Philos. Mag. Lett. 79 (1999) 755.
[15] B.E. Warren, X-ray Diffraction, Addison-Wesley, Reading, MA, 1969.
[16] D.T. Cromer, J.B. Mann, Acta Crystallogr. A 24 (1968) 321.
[17] M. Burman, J. Hirsch, T. Ramdeen, J. Phys. C 14 (1981) 117.
[18] T. Tiedje, J.M. Cebulka, D.L. Morel, B. Abeles, Phys. Rev. Lett. 46 (1981) 1425.
[19] E.R. Whipple, S.N. Subbarao, F.P. Koffyberg, J. Solid State Chem. 34 (1980) 231.
[20] N.F. Mott, E.A. Davis, Electronic Processes in Non-Crystalline Materials, 2nd Ed., Clarendon, Oxford, 1979, p. 161.
[21] N. Kikuchi, H. Hosono, H. Kawazoe, K. Oyoshi, S. Hishita, J. Am. Ceram. Soc. 80 (1997) 22.